THE ASTROPHYSICAL JOURNAL, 449:L149–L152, 1995 August 20

DISCOVERY OF INVERSE-COMPTON X-RAYS IN RADIO LOBES

E. D. FEIGELSON, S. A. LAURENT-MUEHLEISEN, AND R. I. KOLLGAARD
Department of Astronomy and Astrophysics, Pennsylvania State University, University Park, PA 16802

AND

E. B. FOMALONT
National Radio Astronomy Observatory, Edgemont Road, Charlottesville, VA 22903
Received 1995 March 20; accepted 1995 June 8

ABSTRACT

Inverse-Compton (IC) scattering of cosmic microwave background photons into the X-ray band by relativistic electrons in diffuse radio lobes is an obligatory process. We present the strongest evidence to date for the detection of these IC X-rays. They appear in a deep image of the nearby radio galaxy Fornax A (=NGC 1316) obtained with the Position Sensitive Proportional Counter on board the *ROSAT* satellite. The spatial correspondence of the X-ray and radio emission is excellent. The absence of Faraday depolarization in the lobes argues strongly against the possibility that the X-rays are due to an entrained thermal plasma. The detected level of X-rays is somewhat higher than, but consistent with, that expected from the assumption of equipartition between magnetic fields and relativistic electrons in the lobes. This observation provides the first direct estimate of the magnetic field of a radio lobe, $B_{IC} \simeq 2$–3 μG, indicating that the integrated energy output of this active galactic nucleus is near the minimum energy level.

Subject headings: galaxies: magnetic fields — radiation mechanisms: nonthermal — radio continuum: galaxies — X-rays: galaxies

1. INTRODUCTION

The energy required to produce the diffuse radio lobes of radio galaxies and quasars has never been clearly established. The observed radio synchrotron emission scales with the product of the relativistic electron population and the magnetic field strength, while the total energy content requires independent knowledge of the particle and field energies. Astrophysicists traditionally assume minimum energy in the lobes, which implies that the particle and magnetic field energy densities are approximately in equipartition (Burbidge 1956). Lobe energetics can be quantified by the detection of inverse-Compton (IC) X-ray emission, which directly measures the electron population. These X-rays are cosmic microwave background photons scattered to high energies by synchrotron-emitting relativistic electrons. This IC process was once interpreted to be responsible for the entire X-ray background radiation (Hoyle 1965; Bergamini, Londrillo, & Setti 1967; Rees 1967), but to date no clear case for X-rays from any individual radio lobe had been found. We report here *ROSAT* observations of the nearby radio galaxy Fornax A that provides the first convincing evidence for these lobe IC X-rays, at a level consistent with the long-standing hypothesis of minimum energy and particle-field equipartition.

IC scattering in radio lobes is an obligatory process: since the cosmic microwave background radiation should pervade all space, every synchrotron radio structure in the sky should have a corresponding X-ray structure. Although predicted since the beginning of extragalactic X-ray astronomy, no convincing example has yet emerged. The difficulties are the faint X-ray levels expected if equipartition holds and confusion produced by much stronger X-ray–emitting components such as the hot gaseous medium surrounding many radio galaxies. For example, the bright radio galaxy Virgo A = M87 has X-ray features near its outer radio lobes, but these might arise from compression of the intracluster medium by the outflowing lobes (Feigelson et al. 1987). Cygnus A and Perseus A show deficits rather than excesses in X-ray emission near the lobes (Carilli, Perley, & Harris 1994; Böhringer et al. 1993), and searches for IC X-rays from Centaurus A produced negative (Marshall & Clark 1981) or contradictory (Feigelson et al. 1981; Morini, Anselmo, & Molteni 1989) results. Other attempts to find lobe IC X-rays have failed (e.g., Feigelson & Berg 1983; Harris et al. 1995). However, X-rays are seen from the Cyg A hot spots, confirming equipartition expectations at the working surface where the jet hits the intracluster medium (Harris, Carilli, & Perley 1994).

We study the southern radio galaxy Fornax A (= PKS 0320−37 = NGC 1316; $z = 0.0060$) at a distance of 17 Mpc (McMillan, Ciardullo, & Jacoby 1993), the fourth brightest radio source in the sky at low frequencies, specifically because extraneous sources of X-rays near the lobes are absent. NGC 1316 resides in the outskirts of the Fornax Cluster, in a region with little intracluster gaseous medium (Forman, Jones, & Tucker 1985). Our observations were made with the *ROSAT* Positional Sensitive Proportional Counter (PSPC) (Trümper 1983), which has the low background and detector uniformity necessary for the study of faint diffuse X-ray emission. Kaneda et al. (1995) report similar results obtained with the *ASCA* satellite, with higher spectral resolution. A preliminary report of our findings appears in Laurent-Muehleisen et al. (1994).

2. OBSERVATIONS AND DATA ANALYSIS

Fornax A was observed with the *ROSAT* PSPC-B detector during 15 orbits between 1992 January 13 and 1992 January 20, with 25.5 ks on-target exposure. The radio lobes are located approximately 15′ east and west of the galaxy, each a sphere 15′–20′ in diameter (Ekers et al. 1983; Fomalont et al. 1989).

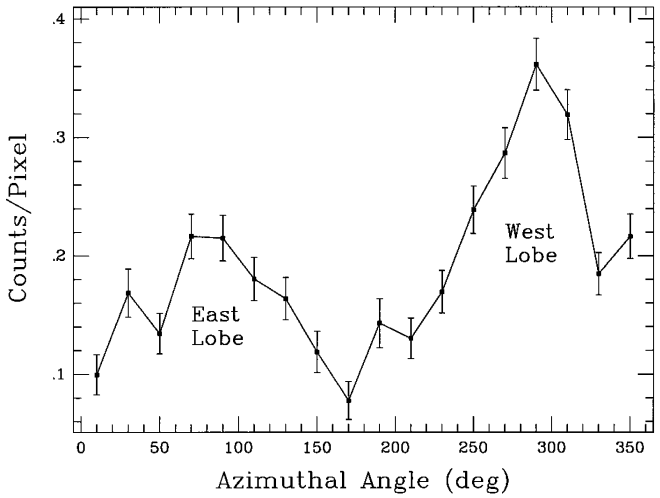

FIG. 1.—Distribution of *ROSAT* PSPC counts per 15″ × 15″ pixel in an annulus between 8′ and 25′ from NGC 1316 in the hard X-ray band 0.9–2.0 keV. Azimuthal angle proceeds east from north, and error bars denote $\sqrt{N}$ counting uncertainties.

The lobes are almost completely enclosed within the unobstructed region of the PSPC detector.

2.1. *Spatial Analysis*

Casual inspection of the image shows a slightly extended source at NGC 1316 (found earlier with the *Einstein Observatory*; Forman et al. 1985) and the usual distribution of weak background sources, but no emission from the lobes. Two data analysis methods were used to reveal the lobe emission, the first simple and the second more sophisticated. Prior to each analysis, events associated with extraneous sources were removed from the image. These included 0.′5–6′ radius circles (depending on location in the detector) around 36 point sources found by standard source detection algorithms, and an 8′ radius circle around NGC 1316. Image analyses were performed in three spectral bands: *C* (0.09–0.42 keV), *M* (0.52–0.91 keV), and *J* (0.91–2.02 keV).

In the first analysis, we examined the distribution of hard *J*-band X-rays in an annulus around the nucleus which includes the lobes centered at P.A. 70° and 285° (Fig. 1). Soft channels are excluded because of the high background rate. X-ray enhancements around the east and west lobes over the off-lobe background are clearly seen. Using a background annular region between 34′ and 40′, we find 2599 (1329) source counts after the removal of 2958 (2131) background counts over an area of 644 (464) arcmin^2 for the west (east) lobe, where the area excludes the removed point sources. The *J*-band lobe count rates are thus 0.179 ± 0.005 (0.252 ± 0.005) counts pixel^{-1}, with errors based on counting statistics. Systematic errors may be present as the background level is poorly defined. The probability that lobe excess is a random fluctuation of the background, assuming Gaussian statistics, is $P < 0.05\%$.

The second analysis draws upon detailed understanding of the contaminating background in the *ROSAT* PSPC detector developed by researchers studying faint diffuse X-ray structures (Snowden & Freyberg 1993; Plucinsky et al. 1993; Snowden et al. 1994). These corrections and analyses were performed using the Interactive Data Language (ver. 3.0.0). Five components of noncosmic background in the PSPC have been identified: particle-induced background, scattered solar X-rays, afterpulsing, short-term enhancements, and long-term enhancements. We eliminated 7% of the exposure due to high particle background (when the detector Master Veto Rate exceeded 170 counts s^{-1}), 35% (75%) of the *C* (*M*) band exposure due to scattered solar X-ray contamination, and 1000 afterpulse events that follow a precursor event by 0.35 ms or less. A three-component spatial, energy, and temporal model for the remaining particle background was computed from the Master Veto Rate and removed from the data. The solar X-ray background was predicted by a model that calculated the scattered solar flux depending on the satellite's orbital orientation each minute. Time intervals when the scattered solar X-rays exceeded 10% of the total flux were removed from further analysis. Vignetting and flat-field corrections were applied using energy-dependent exposure maps. Circular regions around point sources were removed and the resulting gaps replaced by an average of pixels from an annular region with radii $R + 0.5$ to $R + 1.75$ arcmin, where R is the radius of the subtracted region about the point source. The final images were divided into the three bands and smoothed with Gaussian kernels.

The western lobe shows a clear excess X-ray emission in the *M* and *J* bands, while the fainter eastern lobe only shows a definite excess in the *J* band. Figure 2 (Plate L18) shows the smoothed *J*-band image overlaid on a radio image. The hard band image shows a remarkable spatial correspondence between the X-ray emission and the radio lobes, unlike the case of Virgo A in which the structures are offset (Feigelson et al. 1987). We note that the regions between the lobes in Figure 2 have excess emission after subtraction of the background model. Either the entire 20′ region around NGC 1316 may contain diffuse X-ray emission or the local Galactic diffuse X-ray emission is higher than predicted by the background model. The instrumental backgrounds in the *C* and *M* bands are higher than in the *J* band, because of residual scattered solar X-rays and possible spatial variations in the diffuse X-ray background.

2.2. *Spectral Analysis*

The data derived from the second analysis were rebinned into the standard 34 *ROSAT* energy channels for spectral analysis with PROS (ver. 2.3.1) and XSPEC (ver. 8.41). In all fits the column density was fixed at the Galactic value $N_{\rm H} = 2.06 \times 10^{20}$ cm^{-3} (Stark et al. 1992). Simple power-law models are consistent with the spectrum of the western lobe, although the inferred index is very uncertain and depends on the energy band examined. The *C*- and *M*-band data suffer considerable particle contamination and an unknown contribution of Galactic diffuse X-ray emission. Using all channels (0.1–2.0 keV), the western lobe has $\alpha_X = -0.8 \pm 0.2$ ($\chi_r^2 = 1.5$ with $r = 27$ and two free parameters), where α_X is the energy spectral index ($S \propto \nu^{+\alpha}$). If the *C* band is omitted, the fit quality is improved but with a steeper spectral index $\alpha_X = -2.1 \pm 0.4$ ($\chi_r^2 = 1.2$ with $r = 16$). Spectral fits for the eastern lobe also give steep spectral indices $\alpha_x \simeq 2$, but this is determined by a large count rate in the *C* band in which residual background fluctuations are large. Omitting the *C*-band channels gives $\alpha_X = 0.0 \pm 1.5$ ($\chi_r^2 = 0.6$ with $r = 16$).

Thermal models using a Raymond-Smith plasma also give satisfactory fits. The western lobe is consistent with $kT = 0.8 \pm 0.1$ keV and electron densities $n_e = 4 \times 10^{-4}$ cm^{-3} ($\chi_r^2 = 1.1$ with $r = 16$). Following our *ROSAT* observations, X-ray emission from the lobes was also detected with *ASCA*

PLATE L18

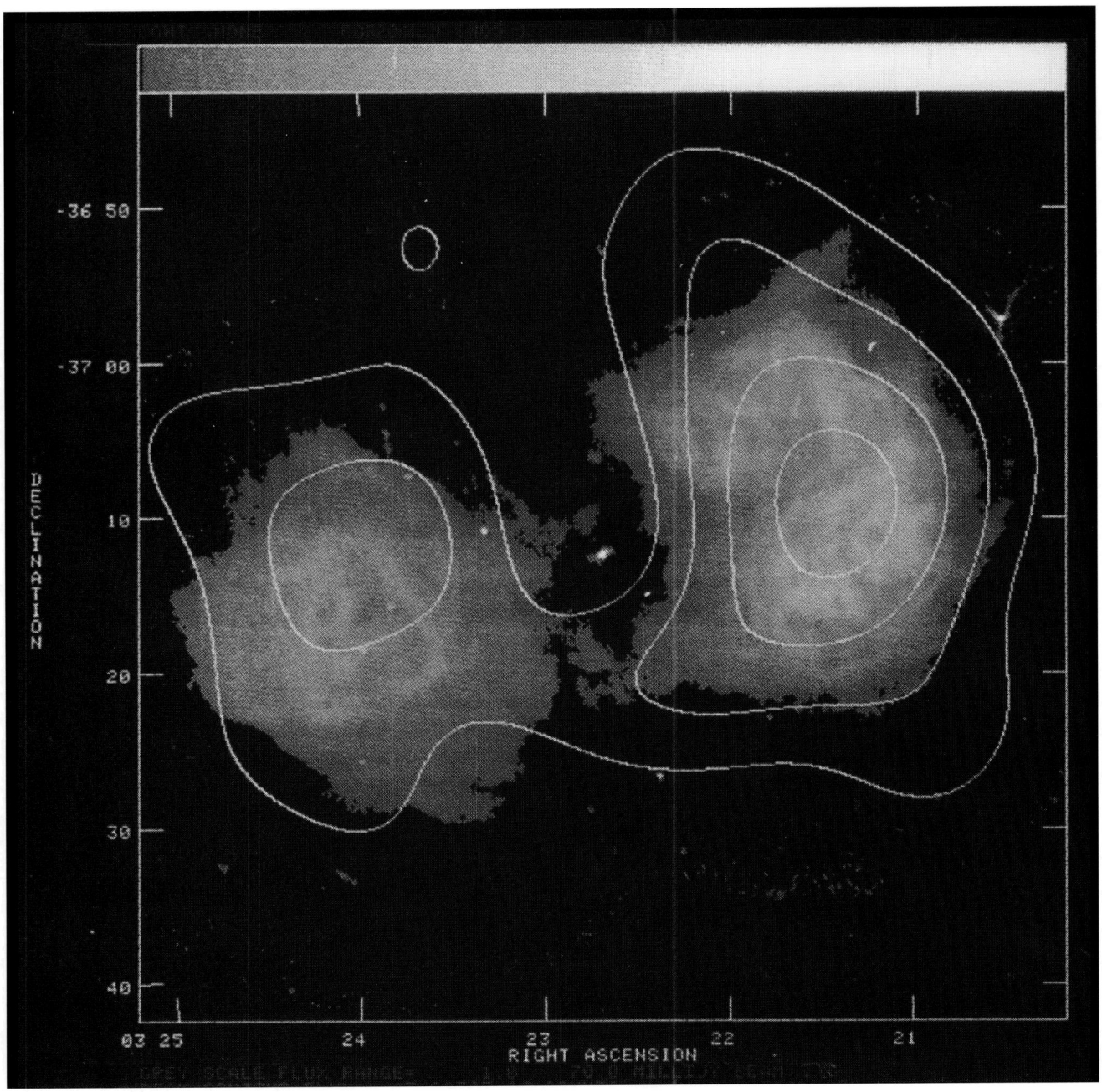

FIG. 2.—Contour map of the PSPC image in the hard 0.9–2.0 keV band after removal of several background components and smoothing with a 5′ FWHM Gaussian kernel. Contours are drawn at 65%, 75%, 85%, and 95% of the peak of 3.1×10^{-6} counts s^{-1} $pixel^{-1}$. The gray-scale image is the 1.4 GHz map obtained at the Very Large Array (Fomalont et al. 1989).

(Kaneda et al. 1995). The *ASCA* data suggest the presence of both a power-law and a thermal component. We find that the *ROSAT* data for the western lobe are consistent with this model. Assuming a fixed spectral index $\alpha_X = -0.9$, the value found by *ASCA*, the best fit has a plasma temperature $kT = 0.7 \pm 0.2$ keV ($\chi_r^2 = 1.1$ with $r = 17$), consistent with $kT = 0.95$ keV found by *ASCA*. The contribution of the power-law component is poorly constrained by the *ROSAT* data in these two-component models.

Radio data provide additional constraints because thermal plasma entrained in the lobe should produce Faraday depolarization of the radio emission. This is not seen. Polarimetric observations from the NRAO Very Large Array show that, except for two localized regions with foreground ionized material, the lobes show no depolarization between 1.4 and 5 GHz, with a polarization fraction $f \simeq 20\%$–30% at both frequencies (Fomalont et al. 1989; E. B. Fomalont, unpublished). At 0.33 GHz, inhomogeneous depolarization is seen, with the east lobe showing $f \simeq 15\%$ and the west lobe $0 < f < 15\%$. The lobe polarization fraction thus drops by half around 0.6–1.0 GHz. Choosing a conservative value of $\langle B \rangle = 3$ μG aligned along the line of sight and using the Faraday depolarization theory for a uniform spherical lobe (Cioffi & Jones 1980), we calculate that a uniformly distributed entrained thermal plasma must have density $n_e \leq 1 \times 10^{-4}$ cm^{-3}. This is severalfold below the density required to provide the observed lobe X-rays by thermal processes.

We conclude that, while the lobe X-ray spectrum from the *ROSAT* data is very uncertain, it may be consistent with a purely IC origin and is definitely consistent with a mixture of IC emission and a soft thermal component as found by Kaneda et al. (1995) from *ASCA* data. The thermal material, if present, must be external to the lobe where it causes no depolarization. Also, the spatial distribution of 0.9–2.0 keV X-rays (Fig. 2) does not show edge-brightening or emission beyond the extent of the radio lobe, which argues against a strong contribution from thermal emission around the lobes in this band. If all of the *ROSAT* lobe emission is attributed to the IC process, its flux density at 1 keV is 0.17 μJy, with a $\pm 30\%$ range due to the uncertainty in the spectral index. If thermal plasma is present, the nonthermal IC flux density may be as low as 0.05–0.10 μJy.

3. DISCUSSION

The IC magnetic field, $B_{\rm IC}$, required to produce a measured ratio of radio to X-ray flux is given by (Harris & Grindlay 1979):

$$B_{\rm IC} = \left[\frac{(4790)^{\alpha_r} C(\alpha_r) G(\alpha_r)(1+z)^{3-\alpha_r} S_r E_x^{\alpha_r}}{10^{70} S_x \nu^{\alpha_r} \sin\phi}\right]^{1/(1-\alpha_r)},$$

where α_r is the radio spectral index, z is the redshift, ϕ is the angle between the uniform magnetic field and the line of sight, S_r is the radio flux density (in janskys) at ν_r (GHz), and S_x is the X-ray flux density (ergs s^{-1} cm^{-2} Hz^{-1}) at energy E_x (keV). The functions $C(\alpha_r)$ and $G(\alpha_r)$ are given by Harris & Grindlay (1979).

This field strength can be compared to the minimum energy field strength (Miley 1980):

$$B_{\rm ME} = 5.69 \times 10^{-5} \times \left[\frac{(1+k)}{\eta}(1+z)^{3-\alpha_r} \frac{1}{\theta^2 s \sin^{3/2}\phi} \frac{S_r}{\nu_r^{\alpha_r}} \frac{\nu_2^{\alpha_r+(1/2)} - \nu_1^{\alpha_r+(1/2)}}{\alpha_r + \frac{1}{2}}\right]^{2/7},$$

TABLE 1

CALCULATED WEST LOBE MAGNETIC FIELD STRENGTH

η	ϕ (rad)	ν_1 (GHz)	k	$B_{\rm ME}$ (μG)	$B_{\rm IC}$ (μG)	$B_{\rm ME}/B_{\rm IC}$
1	$\pi/2$	10^{-2}	1	3.0	1.7	1.7
1	0.17	10^{-2}	1	6.3	4.6	1.4
1	$\pi/2$	10^{-4}	1	4.5	1.7	2.6
1	$\pi/2$	10^{-2}	100	9.1	1.7	5.2
0.1	$\pi/2$	10^{-2}	1	5.7	1.7	3.3
0.01	$\pi/2$	10^{-2}	1	11.0	1.7	6.4

NOTE.—The calculation is based on the following: $\alpha_r = -0.8$, $S_r = 74$ Jy at $\nu_r = 1.4$ GHz, $\theta = 1020''$, and $s = 74$ kpc are derived from low-frequency synchrotron observations (Ekers et al. 1983). Fitting a $\alpha_x = -0.8$ power-law model with Galactic foreground $N_{\rm H} = 2 \times 10^{20}$ cm^{-2} to the west lobe excess gives $S_x = 1.7 \times 10^{-30}$ ergs s^{-1} cm^{-2} Hz^{-1} at $E_x = 1$ keV. The upper synchrotron cutoff is taken to be $\nu_2 = 100$ GHz.

where k is the ratio of the energy in heavy particles to the energy in electrons, η is the filling factor of the synchrotron emitting region, θ is the lobe diameter in arcseconds, s is the path length through the source in kiloparsecs, ϕ is the angle between the (assumed uniform) magnetic field and the line of sight, and ν_1 and ν_2 (GHz) are the upper and lower cutoff frequencies for the radio synchrotron spectrum. While $B_{\rm ME}$ depends on several factors that are not well constrained by observation, the dependence is relatively weak.

Table 1 shows values of $B_{\rm IC}$ and $B_{\rm ME}$ for the west lobe for illustrative values of uncertain parameters. $B_{\rm IC}$ is calculated assuming all of the X-ray emission is due to the IC process. The first row of the table with $\phi = \pi/2$, $\nu_1 = 10$ MHz, and $k = 1$ represents commonly assumed values that give minimum energies in radio lobes. In this case, the observed lobe X-rays are a factor of 2 higher than predicted by simple minimum energy theory. Equivalently, the magnetic field necessary to produce the observed X-rays, $B_{\rm IC} = 1.7$ μG, is a factor of 1.7 below the minimum energy level. If the magnetic field orientation is close to the line of sight (low ϕ), then the inferred field becomes closer to $B_{\rm ME}$. If the particle energies are dominated by protons (high k) or if the particles and fields do not fill the entire lobe (low η), then the lobe is farther from equipartition, and observed X-ray emission can be an order of magnitude higher than that expected from minimum energy arguments. The true field $B_{\rm IC}$ is then 2–5 times weaker than $B_{\rm ME}$, and the total energy density of the lobe (which is $B_{\rm IC}^2/8\pi$ plus the energy in the particles) is an order of magnitude higher than the minimum energy. The detection of strong X-rays from the lobes excludes, for almost all reasonable combination of parameters, the possibility that the magnetic field energy density exceeds that from the particles.

We conclude that the IC interpretation for the Fornax A X-ray lobe emission is quite satisfactory, and the lobe magnetic field appears somewhat weaker than expected from simple minimum energy arguments. This discrepancy would be removed if some of the X-ray emission is from an external thermal plasma, in which case the inferred lobe field strength would rise from $B_{\rm IC} = 1.7$ to 2–3 μG.

One complicating factor should be considered: there is good reason to believe that the magnetic field filling factor η is less than unity. High-resolution radio images of the Fornax A lobes (Fomalont et al. 1989) show strong filamentation in the synchrotron emission. It is thus likely that $\eta < 1$, and $B_{\rm ME}$ is correspondingly increased (Table 1). This filamentation may arise from unstable magnetohydrodynamic perturbations in a

plasma experiencing synchrotron and inverse-Compton losses (e.g., Bodo et al. 1990; Gouveia Dal Pino & Opher 1993). However, it is not clear whether the filamentation is due to concentrations of the relativistic particles, the magnetic field, or both. These possibilities give different predictions for the IC X-ray flux. The physics of inhomogeneous radio lobes would be considerably elucidated if high-resolution X-ray imaging of Fornax A could determine whether the IC X-ray emission (i.e., the particle density alone) as well as the synchrotron emission is filamentary.

4. CONCLUSION

We conclude that Fornax A provides the most convincing case to date for X-ray IC emission from scattering of the cosmic microwave background by relativistic electrons in radio lobes. The spatial coincidence of the X-ray and radio structures is excellent, as required by the IC mechanism. Thermal emission from within the lobes is incompatible with Faraday depolarization observations, although some of the emission may arise from thermal plasma external to the lobes. The X-ray spectrum appears softer than expected from a simple IC model, but the spectral results are very uncertain due to uncertain soft band background subtraction and possible contributions by either Galactic emission or a diffuse plasma around NGC 1316. The observed X-ray level is somewhat above, but largely consistent with, the assumption of minimum energy and equipartition in radio lobes, though we can not exclude the possibility that relativistic particle energy exceeds the magnetic field energy by up to one order of magnitude. Therefore, if Fornax A is representative of radio galaxies in general, the integrated energy output of relativistic particles from radio-loud active galactic nuclei is constrained to be close to their minimum energy levels.

We thank J. A. Mendenhall and D. N. Burrows for their assistance with the PSPC background analysis, K. Makishima for communication of *ASCA* results prior to publication, and the referee for a number of valuable suggestions. This work was supported by NASA grants NAGW-2120 and NAG5-1959. The National Radio Astronomy Observatory is operated by Associated Universities, Inc., under contract with the National Science Foundation.

REFERENCES

Bergamini, R., Londrillo, P., & Setti, G. 1967, Nuovo Cimento, 52B, 495
Bodo, G., Ferrari, A., Massaglia, S., & Trussoni, E. 1990, MNRAS, 244, 530
Böhringer, H., Voges, W., Fabian, A. C., Edge, A. C., & Neumann, D. M. 1993, MNRAS, 264, L25
Burbidge, G. 1956, ApJ, 124, 416
Carilli, C. L., Perley, R. A., & Harris, D. E. 1994, MNRAS, 270, 173
Cioffi, D. F., & Jones, T. W. 1980, AJ, 85, 368
Ekers, R. D., Goss, W. M., Wellington, K. J., Bosma, A., Smith, R. M., & Schweizer, F. 1983, A&A, 127, 361
Feigelson, E. D., & Berg, C. J. 1983, ApJ, 269, 400
Feigelson, E., Schreier, E., Delvaille, J., Giacconi, R., Grindlay, J., & Lightman, A. 1981, ApJ, 251, 31
Feigelson, E. D., Wood, P. A., Schreier, E. J., Harris, D. E., & Reid, M. J. 1987, ApJ, 312, 101
Fomalont, E. B., Ebneter, K. A., van Breugel, W. J., & Ekers, R. D. 1989, ApJ, 346, L17
Forman, W., Jones, C., & Tucker, W. 1985, ApJ 293, 102
Gouveia Dal Pino, E. M., & Opher, R. 1993, MNRAS, 263, 687
Harris, D. E., Carilli, C. L., & Perley, R. A. 1994, Nature, 367, 713
Harris, D. E., & Grindlay, J. E. 1979, MNRAS, 188, 25
Harris, D. E., Willis, A. G., Dewdney, P. E., & Batty, J. 1995, MNRAS, in press
Hoyle, F. 1965, Phys. Rev. Lett., 15, 131
Kaneda, H., et al. 1995, preprint
Laurent-Muehleisen, S., Feigelson, E. D., Kollgaard, R. I., & Fomalont, E. B. 1994 in The Soft X-Ray Cosmos, ed. E. M. Schlegel & R. Petre (New York: AIP), 418
Marshall, F. J., & Clark, G. W. 1981, ApJ, 245, 840
McMillan, R., Ciardullo, R., & Jacoby, G. H. 1993, ApJ, 416, 62
Miley, G. 1980, ARA&A, 18, 165
Morini, M., Anselmo, F., & Molteni, D. 1989, ApJ, 246, 750
Plucinsky, P. P., Snowden, S. L., Briel, U. G., Hasinger, G., & Pfeffermann, E. 1993, ApJ, 418, 519
Rees, M. J. 1967, MNRAS, 137, 429
Snowden, S. L., & Freyberg, M. J. 1993, ApJ, 404, 403
Snowden, S. L., McCammon, D., Burrows, D. N., & Mendenhall, J. A. 1994, ApJ, 424, 714
Stark, A. A., Gammie, C. F., Wilson, R. W., Bally, J., Linke, R. A., Heiles, C., & Hurwitz, M. 1992, ApJS, 79, 77
Trümper, J. 1983, Adv. Space Res., 2, 241